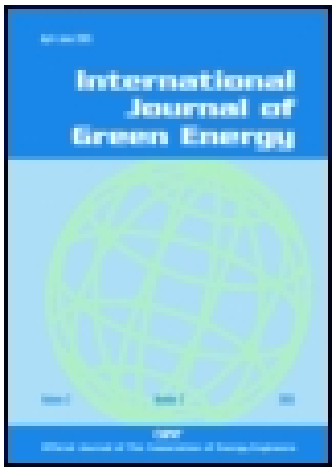

International Journal of Green Energy
Publication details, including instructions for authors and subscription information:
http://www.tandfonline.com/loi/ljge20

A Parametric Study on the Thermal Performance of Unglazed Solar Water Collectors with their Colorbond Steel Absorber Plates also Used as Roofs

Matthew Walsh [a b] & Wenxian Lin [a b]

[a] Solar Energy Research Institute, Yunnan Normal University , Kunming , Yunnan , 650092 , P. R. China

[b] School of Engineering and Physical Sciences , James Cook University , Townsville , QLD 4811 , Australia

Accepted author version posted online: 10 Feb 2014.

To cite this article: Matthew Walsh & Wenxian Lin (2014): A Parametric Study on the Thermal Performance of Unglazed Solar Water Collectors with their Colorbond Steel Absorber Plates also Used as Roofs, International Journal of Green Energy, DOI: 10.1080/15435075.2013.858045

To link to this article: http://dx.doi.org/10.1080/15435075.2013.858045

A PARAMETRIC STUDY ON THE THERMAL PERFORMANCE OF UNGLAZED SOLAR WATER COLLECTORS WITH THEIR COLORBOND STEEL ABSORBER PLATES ALSO USED AS ROOFS

Matthew Walsh[a,b] and Wenxian Lin[a,b,*]

[a] Solar Energy Research Institute, Yunnan Normal University, Kunming, Yunnan 650092, P. R. China

[b] School of Engineering and Physical Sciences, James Cook University, Townsville, QLD 4811, Australia

[*]Author for correspondence: Associate Professor Wenxian Lin, School of Engineering and Physical Sciences, James Cook University, Townsville QLD 4811, Australia. Tel: +61-7-47815091, Fax: +61-7-47816788, e-mail: wenxian.lin@jcu.edu.au

Abstract

In this paper, an innovative unglazed solar water collector with its colorbond steel absorber plate also serving as the roof is proposed. Two most common colorbond steel profiles used as roofs, namely the Lysaght BlueOrb colorbond steel with the cosine profile and the Spandek colorbond steel with a trapezoidal shaped profile, are selected as the absorber plates. A theoretical energy balance model is developed to conduct a detailed parametric study on the

thermal performance of this innovative unglazed solar collector with both colorbond steel absorber plate profiles under various configuration and operating conditions. The results show that both types of collectors can achieve high thermal efficiency (~70%) and can increase the water temperature by about 8 ^{o}C, indicating they are suitable for the domestic utilization in at least tropical and similar regions as well; The two types of collectors produce very close thermal performances; improved thermal performance can be achieved through optimizing a number of parameters such as using a selective coating for the absorber plate to enhance its optical properties, using slender collector configurations, and using a compromised mass flow rate to maintain a high efficiency and to attain the higher temperature outputs.

Keywords: Unglazed solar water collector; Colorbond steel absorber plate; Thermal performance; Energy balance model; Spandek colorbond steel; Lysaght BlueOrb colorbond steel

INTRODUCTION

A world energy crisis has provided a new impetus to the solar energy utilization research and development program on a global scale. Terrestrial solar radiation is a low intensity, variable energy resource that arrives at the Earth's surface at strengths of about 1000 W/m^2 at noon on

clear sunny days. Although solar energy can be utilized for power generation, the terrestrial radiation is more than suitable to also supply homes with readily available hot water.

Solar hot water systems have been studied extensively, with primary goals of collecting the maximum amount of solar energy at a minimalistic cost (Sopian, et al., 2004). Currently the cost effectiveness of this energy system is still doubtful, as the current upfront costs are more expensive than traditional systems (Hassan and Beliveau, 2008). Therefore, more effort is necessary to reduce the module and installation costs. A low energy cost can be obtained by a combination of several steps outlined by Bonhôte, Eperon and Renaud (2009). These steps include integrating long-lived steel-made solar collectors as pieces of the facade, replacing standard covering elements, easy installation, high facade coverage that is aesthetically appealing, coloured coatings of high selectivity and the optimized integration in heating systems.

Currently, all solar hot water heating systems can be identified into two distinct categories, active or passive systems (Rabl, 1985). This division is convenient even though the distinction is not always clear. Active systems use storage units and collectors as two separate components with pumped energy transport, while passive systems rely on natural energy transfer mechanisms such as gravity, without the need for any moving parts. Common active solar hot water systems

include the flat plate, evacuated tube, and concentrating beam solar collectors while common passive systems include the syphoned and heated air powered solar collectors (see, e.g., Duffie and Beckman, 1980; Gillet and Moon, 1985; Thirugnanasambandam, Iniyan and Goic, 2010; Mondol, Smyth and Zacharopoulos, 2011). Many of these systems are glazed using one or more covers, and have been documented extensively (e.g., Belusko, Saman and Bruno, 2004; Juanicó, 2008; Dagdougui, et al., 2011). However, the introduction of glazing increases the upfront and maintenance costs of the system (Sopian, et al., 2004). To counter this, the authors propose an unglazed solar water collector using colorbond steel as its absorber plate which at the same time also serves as the roof.

Limited studies have been done on unglazed solar collectors for household water heating applications. There are several studies on the effectiveness and performance of unglazed solar collectors in slaughterhouses (Chaichana, Kiatsiriroat and Nuntaphan, 2010) and in large scale roofing applications (Medved, Arkar and Černe, 2003; Bonhôte, Eperon and Renaud, 2009). Other studies include comparing the thermal properties of two identical collectors with and without glazing (Chow, et al., 2009), conducting experiments to determine correlations between the wind speed and the wind convection heat transfer coefficient (Kumar and Mullick, 2010),

and investigating the performance of a passive unglazed system constructed from fibreglass polyester reinforcement instead of typical metallic materials (Sopian, et al., 2004; Stojanović, Hallberg and Akander, 2010).

In this paper, a thorough and detailed parametric study is conducted to determine the thermal performance of an unglazed solar water collector which uses colorbond steel as the absorber plate which also functions as the roof. Comparisons is also made between two predominant colorbond steel profiles located in Australia, namely the Lysaght BlueOrb colorbond steel absorber plate with the cosine profile and the Spandek colorbond steel absorber plate with a trapezoidal shaped profile (Colorbond Steel Australia, 2010), to determine which profile produces a better thermal performance.

THEORETICAL ANALYSIS

Two variations of unglazed solar water collectors with their colorbond steel absorber plates also serve as the roofs, called Type 1 and Type 2 collectors for simplicity, are considered in this paper. The colorbond steel absorber plates for both types of collectors have wavelike shaped profiles (Colorbond Steel Australia, 2010), as depicted in Fig. 1. For Type 1 collector, the Lysaght BlueOrb colorbond steel absorber plate with the profile modelled by the cosine function:

$y = 0.008[1 - cos(2\pi x / 0.076)]$ (m) is used, where x and y are the horizontal and vertical coordinates, respectively. For Type 2 collector, the Spandek colorbond steel absorber plate with a trapezoidal shaped profile is used. For both types of collectors, the absorber plate also functions as the roof and is connected to back insulation. Water flows through the channels formed by the back insulation and the absorber plate, where it is heated by the absorbed solar radiation throughout the absorber plate.

(Fig. 1 location)

The aim of this study is to investigate the thermal performance of these two types of collectors by studying the effect that each configuration parameter and operational parameter has on the solar water heating systems formed by these collectors. This determines whether suitable efficiencies and water temperatures can be attained by using these collectors.

To thermodynamically model the solar water collectors described above, some simplifying assumptions, as listed below, should be made to formulate solutions without obscuring the basic physical situation:

- The thermal performance of collectors throughout a day is considered; the time intervals of five minutes are deemed suitable to assume that steady state conditions exist for the considered individual time intervals.
- Thermal losses through the collector backs are predominantly due to conduction across the insulation and the heat flow through the back insulation is one-dimensional and perpendicular to the water flow.
- For each time interval considered, the absorber plate is at the same temperature T_p (mean absorber plate temperature, K); the water temperature inside the channel is at T_f (mean fluid temperature across the section, K) which is uniform across the section that is perpendicular to the flow direction and varies only in the flow direction; the upper surface of the back insulation (which is in direct contact with the water in the channel) is at the same temperature T_f as the water above it, and the bottom surface of the back insulation is at the same temperature T_∞ (K) as the ambient.
- The sky can be considered as a blackbody for long-wavelength radiation at an equivalent sky temperature T_s (K).
- Dust, dirt or rust on the collector and shading of the absorber plate has been neglected.
- An ideal adiabatic storage tank is considered, with no heat loss.

- There are negligible thermal losses through pipework between the collector and the storage tank.
- Thermal inertia of collector components is negligible.
- Flow rates through each channel are considered equal.
- All channels, storage tank and related pipework to and from the collector are free of leakage.

These assumptions and simplifications were successfully used for the analysis of many similar solar collecting devices, such as solar air collectors with v-groove absorber and cross-corrugated absorbers (Lin, Gao and Liu, 2006; Liu, et al., 2007a, 2007b; Gao, et al., 2007).

Energy balance model

To model the unglazed solar water collectors, first the geometry of the absorber plate profile and the energy balance in the collector need to be determined. These are illustrated in Fig. 2 and Fig. 3, along with the relevant parameters. For simplicity, only the BlueScope Lysaght Custom BlueOrb steel absorber plate profile is showcased in these figures.

(Fig. 2 location)

(Fig. 3 location)

It is assumed that the two types of collectors studied in this paper can be approximated by the sheet-tube model (Duffie and Beckman, 1980), as depicted in Fig. 4. The energy balance in these collectors can be represented by a thermal network presented in Fig. 5 and an equivalent thermal network presented in Fig. 6, respectively.

(Fig. 4 location)

(Fig. 5 location)

(Fig. 6 location)

The useful energy gain Q_u for the collector is then determined by (Duffie and Beckman, 1980),

$$Q_u = A_c F_R \left[\alpha_p G - U_L \left(T_{f,i} - T_\infty\right)\right] \quad (1)$$

where U_L is the heat transfer coefficient of the collector (W/m^2·K), F_R is the collector heat removal factor (dimensionless), A_c is the collector area (m^2), and $T_{f,i}$ is the inlet fluid temperature (K).

From Fig. 5, U_L is determined by,

$$U_L = \left(h_w + h_r\right) + \frac{k_i}{t_i} \qquad (2)$$

where h_w, the convection heat transfer coefficient by wind (at a speed u_w), is estimated by (Kumar and Mullick, 2010)

$$h_w = 6.5 + 3.3u_w \qquad (3)$$

and h_r, the radiation heat transfer coefficient from the absorber plate to the ambient, can be written as,

$$h_r = \sigma\varepsilon_p\left(T_p^2 + T_\infty^2\right)\left(T_p + T_\infty\right) \qquad (4)$$

in which ε_p is the absorber plate emittance (dimensionless) and σ is the Stefan-Boltzmann constant ($\sigma = 5.67 \times 10^{-8}$ W/m^2·K^4).

The collector heat removal factor, F_R, is obtained from the fin-theory (Duffie and Beckman, 1980) as

$$F_R = \frac{\dot{m}C_p}{A_c U_L}\left[1 - e^{-\left(\frac{A_c U_L F'}{\dot{m}C_p}\right)}\right] \qquad (5)$$

where $\dot{m}$ is the mass flow rate of the fluid passing through the channels formed by the absorber plate and the top of the back insulation (kg/s, as shown in Fig. 2), C_p is the specific heat of water (J/kg·K), and F' is the collector efficiency factor (dimensionless).

F' is calculated by (Duffie and Beckman, 1980)

$$F' = \left(\frac{W}{D_h + (W - D_h)F} + \frac{WU_L}{\pi D_h h_{f,i}} \right)^{-1} \quad (6)$$

where F is the fin efficiency (dimensionless) and $h_{f,i}$ (W/m^2·K) is the convection heat transfer coefficient between the fluid and the tube wall (see Fig. 4), respectively.

The fin efficiency is determined by the fin-theory (Duffie and Beckman, 1980) as

$$F = \frac{tanh[C_L(W - D_h)/2]}{C_L(W - D_h)/2} \quad (7)$$

where

$$C_L = \sqrt{\frac{U_L}{k_p \delta}} \quad (8)$$

and D_h, the hydraulic diameter of each channel for fluid flow formed by the absorber and the upper surface of the back insulation (as shown in Fig. 4), is calculated by,

$$D_h = \frac{4A_w}{P_w} \quad (9)$$

$h_{f,i}$ can be determined by

$$h_{f,i} = Nu\frac{k_w}{D_h} \quad (10)$$

where k_w (W/m·K) is the thermal conductivity of water and Nu (dimensionless) is the Nusselt number which is calculated by

$$Nu = \frac{3.7 + a\left(\mathrm{Re}\,\mathrm{Pr}\,D_h / L\right)^c}{1 + b\left(\mathrm{Re}\,\mathrm{Pr}\,D_h / L\right)^d} \quad (11)$$

in which Pr is the Prandtl number of water at the inlet fluid temperature (dimensionless), Re is the Reynolds number (dimensionless), and a, b, c and d are constants, which are presented for various Prandtl numbers in Table 1 (Duffie and Beckman, 1980),

(Table 1 location)

The Reynolds number is calculated by,

$$\mathrm{Re} = \frac{u_L D_h}{\nu} \quad (12)$$

where u_L (m/s) is the velocity of water passing the channels and ν (m^2/s) is the kinematic viscosity of water at the inlet fluid temperature.

The collector overall efficiency (dimensionless) is defined as the ratio of useful energy gain to the total solar radiation incident on the collector surface,

$$\eta = \frac{Q_u}{A_c G} \tag{13}$$

The outlet fluid temperature, $T_{f,o}$ (K), and the mean plate temperature, T_p, can be calculated by the following equations (Duffie and Beckman, 1980), respectively,

$$T_{f,o} = T_\infty + \frac{\alpha G}{U_L} + \left(T_{f,i} - T_\infty + \frac{\alpha G}{U_L} \right) e^{\left(-\frac{A_c U_L F'}{\dot{m} C_p} \right)} \tag{14}$$

$$T_p = T_{f,i} + \frac{Q_u}{A_c U_L F_R} \left(1 - F_R \right) \tag{15}$$

Effect of the Storage Tank

To determine the effect a storage tank has on the thermal performance of the solar water collector considered in this paper, the transient response of the solar collector throughout a whole day is analysed. To achieve this, the minutely total solar radiation, ambient temperature, and wind speed have to be used. In this study, the monthly average total solar radiation in Townsville,

Australia, on an hourly basis for each month of a year, as shown in Table 2 (Australian Solar Energy Society, 2006), is used. An interpolation technique is then used to obtain the minutely solar radiation from the monthly solar radiation. Similarly, the monthly average temperature and wind speed in Townsville for each month of a year (Australian Solar Energy Society, 2006), as shown in Table 3 and in Table 4, are used to obtain in the similar manner the required minutely ambient temperature and wind speed for the calculation of the transient response of the solar collector throughout the whole day.

(Table 2 location)

(Table 3 location)

(Table 4 location)

To provide meaningful results, the transient response of the solar collector will be calculated in five minute intervals. This requires an iterative numerical approach to the problem, which will be addressed in Section 2.3. The values of solar radiation, ambient temperature, and wind speed within these much smaller time intervals are obtained by interpolating the available values presented in Tables 2-4 as stated above.

An important component that must be considered in this numerical approach is the inclusion of a water storage tank as it is another major component that a typical solar water heating system must have. Figure 7 shows the schematic of the solar water heating system which consists of the storage tank and the solar collector. At the start of the day (also the start of the calculation), the water inside the storage tank and the collector are assumed to be at the same temperature as the ambient air temperature, T_∞. The heat loss through conduction of the storage tank wall materials and the pipework connecting the collector and the tank are considered to be negligible, which is an appropriate approximation but significantly simplifies the analysis without a considerable impact on the conclusions of this study.

(Fig. 7 location)

Apparently, the collector inlet water temperature $T_{f,i}$ is affected by the temperature of the water leaving the storage tank at the bottom and the temperature of water at the top of the tank is the same as $T_{f,o}$ at time, t (s), throughout the day. The transient distribution of water temperature in a storage tank is quite complicated, as demonstrated recently by Ievers and Lin (2009). To simplify the analysis and calculations, a much simpler "push in – push out" model, as shown in Fig. 8, is proposed to model the vertical distribution of water temperature within the tank. This approach

assumes that the water within the storage tank consists of many small segments with equal sizes (for a five-minute period, the total number of segments is $M_s / 300\dot{m}$), each at a uniform temperature and with the same mass of water ($\dot{m} \times 5$ minutes $= 300\dot{m}$ kg), and there is no mixing or conduction between adjacent segments throughout each five-minute interval of calculation. The mass of each water segment equals to the mass of water that would flow through the solar collector during the five-minute period of calculation. For a specific five-minute interval of calculation, as demonstrated in Fig. 8, a segment of water at $T_{f,o}$, which comes out of the collector outlet and is calculated by using the temperature of the first water segment at the bottom of the tank (i.e., $T_{f,i}$) obtained from previous five-minute interval of calculation, is added to the top of the tank by forced circulation, pushing all water segments in the tank to move down by the same amount, which pushes a segment of water at the bottom of the tank into the inlet of the collector and the temperature of this amount of water becomes $T_{f,I}$ for the next five-minute interval of calculation. Then during the next five-minute interval of calculation, the water coming from the collector with an updated value of $T_{f,o}$ will become the first segment at the top of the tank, pushing the segment that was previously at the top of the tank to become the segment underneath and all other segments in the tank to move down by the same amount and the segment at the bottom of the tank will be pushed out of the tank to become the inlet water for the

collector, with an updated value of $T_{f,i}$. With the time goes on, this process is repeated until the end of the day which is also the end of the calculations.

(Fig. 8 location)

Numerical solution approach

It is apparent that for each five-minute interval of calculation, an iterative approach is necessary to find Q_u, η, $T_{f,o}$, and T_p as they all depend on U_L which in turn depends on T_p, but T_p is unknown *a priori* and is also a parameter that a solution is sought, as represented by eqn (15). First a guess is made of the unknown T_p, from which h_r and then U_L are estimated by eqn (4) and eqn (2), respectively. With this estimated value of U_L and the calculated value of $h_{f,i}$ with eqn (10), F' and F_R can be estimated from eqn (6) and eqn (5), respectively, which then give the estimated values of Q_u, η and $T_{f,o}$, calculated respectively by eqn (1), eqn (13) and eqn (14), and a new value of T_p, obtained from eqn (15). With this new value of T_p, a new iteration is carried out and the process is repeated until all solutions are converged.

A Maltab code using this iterative numerical approach and the equations presented in Section 2.1 is developed to obtain the solutions for all cases considered in this paper.

RESULTS AND DISCUSSION

A comprehensive parametric study is conducted in this section to examine the thermal performances of both types of solar water collectors under various configurations and operating conditions. The configuration parameters of the collectors considered here are W, L, n, D, t_i, k_i, δ, k_p, M_s, ε_p and α_p, and the operating parameters are G, θ, $\dot{m}$ and $T_{f,i}$, respectively. It is apparent that η, $T_{f,o}$, $\Delta T_f = T_{f,o} - T_{f,i}$ which is the temperature rise of fluid passing through the channels, and T_p are appropriate parameters to characterize the thermal performance of the collectors.

Before the study of individual parameter on the thermal performance of the collectors, it is worthwhile to obtain the results under typical configurations and operating conditions to get an overall picture of the collectors' performance.

All simulations are conducted using the Matlab code which is compiled using the methods shown in Section 2, as stated above.

Results under typical configurations and operating conditions

Under typical configurations and operating conditions, the following values are used for their corresponding parameters: G = 700 W/m^2, L = 2 m, n = 20, t_i = 0.1 m, k_i = 0.045 W/m·K, δ =

0.42 mm, k_p = 55 W/m·K, ε_p = 0.11, α_p = 0.95, $\dot{m}$ = 0.05 kg/s, T_∞ = 298 K, $T_{f,i}$ = 298 K and h_w = 14.75 W/m^2·K. For the Type 1 collector, A_w = 540 mm^2, P_w = 151.32 mm and W = 76 mm. For the Type 2 collector, A_w = 864.42 mm^2, P_w = 136.82 mm and W = 87.5 mm.

Under typical configurations and operating conditions, the calculated thermal performances of both collectors are summarized in Table 5. From this table, it is found that both types of collectors can achieve high thermal efficiency (~70%) and can increase the water temperature by about 8 ^{o}C, which is basically adequate for the domestic utilization in the North Queensland where the yearly average ambient temperature is over 25 ^{o}C. It is also found that Type 2 collector outperforms Type 1 collector in terms of thermal performance and efficiencies. This is expected as a larger cross sectional area and larger spacing between the tubes are apparent for Type 2 collector. However this improvement is very marginal, which is also true for all other cases considered, as will be shown subsequently.

(Table 5 location)

It should be noted that in the above numerical calculation, no heat exchanger is included for simplicity. However, a heat exchanger will most likely be used in practical applications to exchange the heat gain obtained from the collector to the water body in the storage tank. If such

a heat exchanger is used, the water temperature rise by about 8 ^{o}C as obtained above will be reduced due to the efficiency of the heat exchanger. Hence, the calculation obtained above and all subsequent numerical calculations are for ideal cases in which no heat changers are involved (or it is assumed that the efficiency of the heat exchangers is 100%). It is apparent that further studies are needed to investigate the effect of the heat exchanger efficiency but this is beyond the scope of the current study. Furthermore, all numerical calculations conducted by this study assume that no hot water consumption load is applied during the heating period, which is the case for most practical applications. However, there are also cases in which hot water consumption loads will be engaged during the heating period. In these cases, specific hot water consumption loads must be taken into account in the numerical calculations and the outcomes are expected to be significantly different. Nevertheless, this is again beyond the scope of the current study and will be the subject for our further studies.

Results under various configurations

The configuration parameters highlighted earlier are W, L, n, D, t_i, k_i, δ, k_p, M_s, ε_p and α_p. Among these parameters, it is obvious that large values of t_i and k_p and smaller values of k_i will result in higher collector efficiencies for both types of collectors considered. It is beyond of the scope of

this study to analyse the effects of δ, W and D as they are specific to the prevailing colorbond steel profiles on the market. Further, it is only necessary to analyse the effects of either n or L as both of these factors influence the absorber surface area A_c. Therefore, only the results for the configuration parameters ε_p ,α_p, M_s and n will be presented here to show their individual effects on the thermal performances of both collectors.

It should be noted that when a specific parameter is chosen to be investigated by changing its value in a reasonable range to see its effect on the thermal performance of both types of collectors, all other parameters will take the values used in the typical configurations and operating conditions as identified in Section 3.1 above.

Effect of ε_p. The results showing the effect of ε_p, the emissivity of thermal radiation of the absorber plate, on the thermal performance of the solar collectors are illustrated in Fig. 9, where ε_p changes in the range of 0.01-1.

(Fig. 9 location)

From the results it is apparent that ε_p does not affect the thermal efficiency of both types of collectors. ε_p is also found to have a negligible effect on the outlet fluid temperature and the

temperature rise for Type 2 collector, although $T_{f,o}$ and ΔT_f slightly decrease with increasing ε_p. It is further observed that Type 2 collector has higher outlet fluid temperatures and temperature rises for all values of emittance investigated. But these improvements are again only marginal, with the efficiency of Type 2 collector even being inferior to Type 1 collector. This is expected as for the same number of parallel tubes, Type 2 collector occupies a larger collector area. The larger hydraulic diameter, D_h, and width between each channel, W, in Type 2 collector also appears to provide this collector with higher temperatures. When increasing ε_p, it is found that the absorber plate temperature for both types of collectors, as expected, decreases monotonically at small rates, although Type 1 collector decreases marginally whereas Type 2 collector decreases much more significantly. These trends are expected as a linear relationship exists between ε_p, h_r and the effect of blackbody radiation from the absorber plate. Therefore increasing ε_p will increase the overall heat loss from the collector through radiation. However, ε_p has a negligible effect on the convection heat transfer between the absorber plate and the ambient.

Therefore, it is ideal to allow the emissivity of thermal radiation from the colorbond steel absorber plates for both types of collectors to be as small as possible. This can be achieved by using a selective coating with very low emittance of thermal radiation.

Effect of α_p**.** Fig. 10 shows the results of the effect of α_p, the absorptivity of solar radiation of the absorber plate, on the thermal performance of the solar collectors, where α_p changes in the range of 0.01-1.

(Fig. 10 location)

From this figure, it is clear that α_p has a dominant effect on the thermal performance of both types of collectors. When α_p increases, all thermal performance parameters, including the thermal efficiency, the outlet fluid temperature, the temperature rise, and the absorber plate temperature, increase almost linearly. This is expected as the absorbed solar radiation on the absorber plate is proportional to α_p. It is also found that Type 2 collector has higher outlet fluid temperatures and temperature rises than Type 1 collector for all values of absorptivity investigated, although the improvements are only marginal again, due to the same reason as discussed in Section 3.2.1 for the case of ε_p. Nevertheless, the efficiencies of both types of collectors are found to be almost identical, indicating that α_p has a negligible effect on the radiation heat transfer between the absorber plate and the ambient, which is confirmed by the results showing in Fig. 10 for T_p where almost identical absorber plate temperatures are found for both types of collectors for each α_p value considered.

Therefore, the absorptivity of solar radiation of the colorbond steel absorber plates for both types of collectors should be as large as possible. This can be achieved by using a selective coating with a very high absorptivity of solar radiation.

Effect of n. The results showing the effect of *n*, the number of parallel fluid channels in the collectors, on the thermal performance of both types of collectors are presented in Fig. 11, where *n* changes in the range of 5-100.

(Fig. 11 location)

It is found that the thermal efficiencies of both types of collectors decrease monotonically when *n* increases, whereas the outlet fluid temperature, the temperature rise, and the absorber plate temperature all increase monotonically with increasing *n*. The amounts of increases or decreases of these parameters with increasing *n* are significant. It is further observed that Type 2 collector, as before, provides higher outlet fluid temperatures and temperature rises for all *n* values investigated. The efficiency of Type 2 collector is almost identical to that of Type 1 collector for each value of *n*. As *n* is identical for both collectors, the mass flow rate through each channel is identical, and the absorber plate area is slightly larger for Type 2 collector. These phenomena help explain the almost identical efficiencies, but again, this affect could be limited to the typical

configuration and operating parameters chosen. When *n* is less than 35, Type 1 collector has a slightly higher absorber plate temperature than Type 2 collector, but when *n* is larger than 35, it becomes the opposite, and the difference in the absorber plate temperature for both types of collectors increases with increasing *n*.

Therefore, it is ideal to prevent the solar collector from having too many parallel tubes to maintain a higher efficiency. This helps reduces the heat loss through radiation and convection on the absorber plate. To accommodate the loss in fluid outlet temperature when decreasing the number of parallel channels, the collector should be constructed to have a slender configuration such that the length of the collector, *L,* is greater than the width, which is affected by the number of parallel tubes.

Effect of M_s. To demonstrate the effect of M_s, the mass of water stored in the storage tank, on the thermal performance of the solar collectors, the time series of $T_{f,i}$, $T_{f,o}$, η, and ΔT_f are calculated based on the five-minute interval modelling through interpolating the monthly average daily solar radiation on a hour basis for January in Townsville, as shown in Table 2. The results are illustrated in Fig. 12 and Fig. 13 for Type 1 and Type 2 collectors respectively, where M_s changes in the range of 100-800 kg.

(Fig. 12 location)

(Fig. 13 location)

When comparing both types of collectors, the results show that smaller storage tank capacities provide higher fluid inlet temperatures and higher fluid outlet temperatures, but smaller temperature rises and efficiencies throughout the day. When the size of the storage tank continued to increase however, the changes of these performances become smaller.

The storage tank had no effect on the convection or radiation heat transfer losses of the solar collector, and its primary purpose is to control the inlet fluid temperature of the collector operating at a specified mass flow rate. It is optimal to select a larger storage tank which allows the inlet fluid temperature to remain closer to the ambient air temperature, as low values of $T_{f,i}$ increase the thermal efficiency of the collectors.

Results under various operating conditions

The operational parameters highlighted earlier are G, θ, $\dot{m}$ and $T_{f,i}$. As the angle the solar collector is positioned towards the sun only influences the amount of solar radiation that can be absorbed by the collector at any given time, it unnecessary to investigate the effect of both G and

θ on the instantaneous thermal performance of the solar collector. Also, it is apparent that the solar collector will attain better thermal performance under a larger G, hence it is unnecessary to investigate the effect of G. Thus, only the results for the operational parameters $\dot{m}$ and $T_{f,i}$ will be presented here to show their individual effects on the thermal performances of both types of collectors.

Effect of $\dot{m}$. The results showing the effect of $\dot{m}$, the fluid mass flow rate, on the thermal performance of the solar collector are illustrated in Fig. 14, where $\dot{m}$ changes in the range of 0.001-0.1 kg/s.

(Fig. 14 location)

From the results it is found that Type 2 collector provides slightly superior performances than Type 1 collector, as demonstrated by a marginally higher outlet fluid temperatures and temperature rises as well as efficiency for all $\dot{m}$ investigated. This is again expected as discussed above. When increasing $\dot{m}$, it is found that the outlet fluid temperatures, absorber plate temperatures and temperature rises decrease monotonically but dramatically for both types of collectors, although with gradually reducing rates of change when $\dot{m}$ is further increased.

However, increasing values of $\dot{m}$ leads to favourable effect on the efficiencies of both types of collector as the efficiencies increases monotonically and considerably with an increase in $\dot{m}$. These trends are expected as efficiency is directly proportional to the product of $\dot{m}$ and ΔT_f. Although the increase of $\dot{m}$ results in the decrease of ΔT_f as observed above, nevertheless, the extent of increase in $\dot{m}$ surpasses the extent of the decrease of ΔT_f, with the ultimate increase of the efficiency with increased $\dot{m}$. As the increase of $\dot{m}$ leads to less time for the heated fluid to pass through the channels, the convection heat transfer between the fluid and absorber plate will be enhanced, resulting in lower absorber plate temperatures, as confirmed by the results shown in Fig. 14(d), which also contributes to the improvement of the efficiency with increased $\dot{m}$.

It is apparent that the mass flow rate, among all parameters studied, has the largest effect on the thermal performance of both types of collectors. To achieve an optimal thermal performance of both types of collectors, a compromised choice of the mass flow rate has to been made by maintaining a high efficiency but at the same time to attain the desired, usually high temperature outputs.

Effect of $T_{f,i}$. From eqn (1) and eqn (13), it is apparent that the thermal performance of both types of collectors are under the influence of $T_{f,i}$, the inlet fluid temperature of the collectors

coming from the storage tank. The results showing this influence are illustrated in Fig. 15, where $T_{f,i}$ changes in the range of 280-360 K.

(Fig. 15 location)

From the results, again it is found that both types of collectors have almost identical thermal performance behaviour although Type 2 collector produces marginally higher temperature rises. The efficiencies of both types of collectors are almost identical. This is expected as the difference in temperatures from the inlet fluid temperature and ambient air temperatures are identical for both types of collectors, as shown by eqn (1). When $T_{f,i}$ increases, it is found that the outlet fluid temperatures increase and temperature rises decrease, both linearly and significantly for both types of collectors. It is also found that increasing in $T_{f,i}$ causes the efficiencies of the collectors to decrease linearly and significantly, which is the result of larger radiation heat loss through the absorber plate and larger conduction heat loss through the back insulation due to higher absorber plate temperatures, as confirmed by Fig. 15(d). Above a certain inlet temperature, the efficiencies begin to drop to below zero and the collectors cease to produce any useful heat for the storage tank and end applications at all, which is of course an undesired outcome.

It is therefore beneficial to maintain $T_{f,i}$ not larger than the ambient air temperature to attain the best thermal performance for both types of collectors.

CONCLUSIONS

The major conclusions from this detailed and thorough parametric study on the thermal performance of the innovative unglazed solar collector with its colorbond steel absorber plate also serving as the roof under various configuration and operating conditions can be summarized as follows:

(1) Both types of collectors can achieve high thermal efficiency (~70%) and can increase the water temperature by about 8 ^{o}C, which is basically adequate for the domestic utilization in the North Queensland where the yearly average ambient temperature is over 25 ^{o}C, indicating these innovative low-cost unglazed solar collectors are suitable for the domestic utilization in at least tropical regions and other similar regions as well.

(2) Generally speaking, Type 2 collector with the trapezoidal shaped profile Spandek colorbond steel absorber plate has a slightly superior configuration than Type 1 collector which has the cosine profile Lysaght BlueOrb colorbond steel absorber plate. This is partly due to the larger cross sectional area and hydraulic diameter of Type 2 collector. Nevertheless, the

differences in thermal performance between these two types of collectors are very marginally for all parameters under investigation.

(3) Improved thermal performance can be achieved for both types of collector through optimizing a number of parameters. For example, a selective coating should be used for the colorbond steel absorber plate to enhance its optical properties by increasing the absorptivity of solar radiation and decreasing the emittance of thermal radiation; The configuration of the collector should also be slender, such that the overall width was much less than the length of the collector; A compromised mass flow rate has to be selected by maintaining a high efficiency and at the same time to attain the desired, usually high temperature outputs; It is beneficial to maintain the inlet fluid temperature of the collector as close as possible to the ambient air temperature by selecting a larger storage tank.

It should be noted that in all numerical calculations carried out by this study, no heat exchanger is included for simplicity, which are valid only for ideal cases. The thermal performance will be reduced if a heat exchanger is used in the system and the effect of the heat exchanger efficiency should be further studied which is beyond the scope of the current study. This study also assumed that no hot water consumption load is applied during the heating period. Again further

studies are required to investigate the effect of hot water consumption loads if they are engaged during the heating period.

ACKNOWLEDGEMENTS

The support from the National Natural Science Foundation of China (11072211), the Natural Science Foundation of Yunnan Province (2011FA017), the Specialized Research Fund for the Doctoral Program of Higher Education (20105303110001), the Program for Changjiang Scholars and Innovative Research Team in University of Ministry of Education of China, and the Australian Research Council is gratefully acknowledged.

NOMENCLATURE

a, b, c, d	constants (-)
A_c	collector area (m^2)
A_w	cross sectional area of each channel (m^2)
C_L	$C_L = (U_L/k_p/\delta)^{1/2}$ (1/m)
C_p	specific heat of water (J/kg·K)

D_h	hydraulic diameter of each channel (m)
F	fin efficiency (-)
F_R	collector heat removal factor (-)
F'	collector efficiency factor (-)
G	solar radiation incident on the solar collector per unit area (W/m^2)
h_b	conduction heat loss coefficient through the back insulation ($W/m^2 \cdot K$)
$h_{f,i}$	convection heat transfer coefficient between the fluid and the tube wall ($W/m^2 \cdot K$)
h_r	radiation heat transfer coefficient from the absorber plate to the ambient ($W/m^2 \cdot K$)
h_w	convection heat transfer coefficient by wind ($W/m^2 \cdot K$)
k_i	thermal conductivity of back insulation (W/m·K)
k_p	thermal conductivity of the colorbond steel absorber plate (W/m·K)

k_w	thermal conductivity of water (W/m·K)
L	length of each channel (m)
m	index for segments in the "push in – push out" model (-)
$\dot{m}$	mass flow rate of the fluid passing through the channels (kg/s)
M_s	total mass of water in the storage tank (kg)
n	number of parallel fluid channels in the collector (-)
Nu	Nusselt number (-)
P_w	wetted perimeter of each channel (m)
Pr	Prandtl number (-)
Q_u	collector useful energy gain (W)
R_1, R_2	thermal resistances between the plate and the sky (m^2·K/W)
Re	Reynolds number (-)
t	time (s)

t_i	thickness of back insulation (m)
T_{f}	water temperature inside the channel (K)
$T_{\mathrm{f,i}}$	inlet fluid temperature (K)
$T_{f,i}^{m}$	water temperature at segment m (K)
$T_{f,o}$	outlet fluid temperature (K)
T_{p}	mean absorber plate temperature (K)
T_{s}	equivalent sky temperature (K)
T_{∞}	ambient air temperature (K)
u_w	average wind speed (m/s)
u_L	velocity of water passing the channels (m/s)
U_{L}	collector heat transfer coefficient ($\mathrm{W/m^2 \cdot K}$)
W	width of each channel (m)
x, y	horizontal and vertical coordinates (m)

Greek symbols

α_p	absorptivity of the absorber plate (-)
δ	thickness of the colorbond steel absorber plate (m)
ε_p	absorber plate emittance (-)
η	collector overall efficiency (-)
θ	inclination angle of the absorber plate to the horizontal (^{o})
ν	kinematic viscosity of water (m^2/s)
σ	Stefan-Boltzmann constant ($\sigma = 5.67 \times 10^{-8}$ $W/m^2 \cdot K^4$)
ΔT_f	$\Delta T_f = T_{f,o} - T_{f,i}$

REFERENCES

Australian Solar Energy Society. (2006). *Australian Solar Radiation Data Handbook* (4th Ed). Canberra, Australia: Australian Governing Funding Service.

Belusko, M., Saman, W., Bruno, F. (2004). Roof integrated solar heating system with glazed collector. *Solar Energy* 76: 61-69.

Bonhôte, P., Eperon, Y., Renaud, P. (2009). Unglazed coloured solar absorbers on façade: Modelling and performance evaluation. *Solar Energy* 83: 799-811.

Chaichana, C., Kiatsiriroat, T., Nuntaphan, A. (2010). Comparison of conventional flat-plate solar collector and solar boosted heat pump using unglazed collector for hot water production in small slaughterhouse. *Heat Transfer Engineering* 31: 419-429.

Chow, T., Pei, G., Fong, K., Lin, Z. Chan, A., Ji, J. (2009). Energy and exergy analysis of photovoltaic-thermal collector. *Applied Energy* 86: 310-316.

Colorbond Steel Australia. (2010). http://www.colorbond.com/. Accessed on 3 May 2011.

Dagdougui, H., Ouammi, A., Robba, M., Sacile, R. (2011). Thermal analysis and performance optimization of a solar water heater flat plate collector: Application to Tétouan (Morocco). *Renewable and Sustainable Energy Reviews* 15: 630-638.

Duffie, J., Beckman, W. (1980). *Solar Engineering of Thermal Processes*. New York: John Wiley & Sons.

Gao, W., Lin, W., Liu, T., Xia, C. (2007). Analytical and experimental studies on the thermal performances of cross-corrugated and flat-plate solar air collectors. *Applied Energy* 84: 425-441.

Gillet, W., Moon, J. (1985). *Solar Collectors: Test Methods and Design Guidelines*. Dordrecht, Netherlands: D. Reidel Publishing Company.

Hassan, M., Beliveau, Y. (2008). Modelling of an integrated solar system. *Building and Environment* 43: 804-810.

Ievers, S., Lin, W. (2009). Numerical simulation of three-dimensional flow dynamics in a hot water storage tank. *Applied Energy* 86: 2604-2614.

Juanicó, L. (2008). A new design of roof-integrated water solar collector for domestic heating and cooling. *Solar Energy* 82: 481-492.

Kumar, S., Mullick, S. (2010). Wind heat transfer coefficient in solar collectors in outdoor conditions. *Solar Energy* 84: 956-963.

Lin, W., Gao, W., Liu, T. (2006). A parametric study on the thermal performance of cross-corrugated solar air collectors. *Applied Thermal Engineering* 26: 1043-1053.

Liu, T., Lin, W., Gao, W., Luo, C., Li, M., Zheng, Q., Xia, C. (2007a). A parametric study on the thermal performance of a solar air collector with a v-groove absorber. *International Journal of Green Energy* 4: 601-622.

Liu, T., Lin, W., Gao, W., Xia, C. (2007b). A comparative study on the thermal performance between a cross-corrugated and a v-groove solar air collector. *International Journal of Green Energy* 4: 427-451.

Medved, S., Arkar, C., Černe, B. (2003). A large-panel unglazed roof-integrated liquid solar collector – energy and economic evaluation. *Solar Energy* 75: 455-467.

Mondol, J., Smyth, M., Zacharopoulos, A. (2011). Experimental characterisation of a novel heat exchanger for a solar hot water application under indoor and outdoor conditions. *Renewable Energy* 36: 1766-1779.

Rabl, A. (1985). *Active Solar Collectors and Their Applications*. Oxford, UK: Oxford University.

Sopian, K., Syahri, M., Abdullah, S., Othman, M.Y., Yatim, B. (2004). Performance of a non-metallic unglazed solar water heater with integrated storage system. *Renewable Energy* 29: 1421-1430.

Stojanović, B., Hallberg, D., Akander, J. (2010). A steady state thermal duct model derived by fin-theory approach and applied on an unglazed solar collector. *Solar Energy* 84: 1838-1851.

Thirugnanasambandam, M., Iniyan, S., Goic, R. (2010). A review of solar thermal technologies. *Renewable and Sustainable Energy Reviews* 14: 312-322.

Fig. 1. The profiles and dimensions of the colorbond steel absorber plates for the two types of solar water collectors considered in this paper [22]: (a) Type 1 collector, with the Lysaght BlueOrb colorbond steel absorber plate having a cosine shaped profile, (b) Type 2 collector, with the Spendek colorbond steel absorber plate having a trapezoidal shaped profile, (c) dimensions of the absorber plate profile for Type 1 collectors, and (d) dimensions of the absorber plate profile for Type 2 collectors.

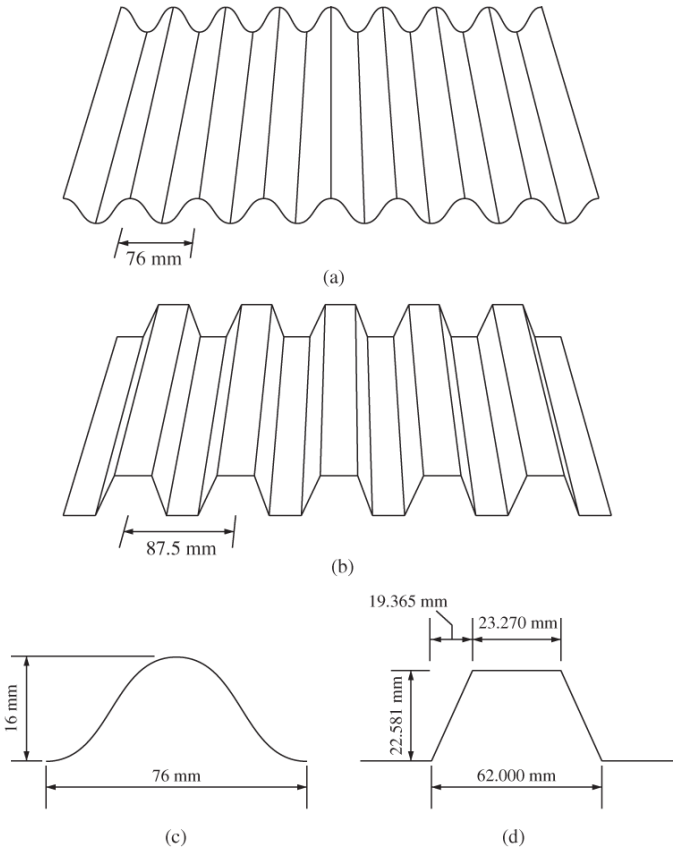

Fig. 2. The cross section (a) and the isometric cross section (b) of the Lysaght BlueOrb colorbond steel collector. L (m) and W (m) are the length and width of each channel, k_p (W/m·K) and δ (m) are the thermal conductivity and thickness of the colorbond steel absorber plate, k_i (W/m·K) and t_i (m) are the thermal conductivity and thickness of back insulation, P_w (m) and A_w (m^2) are the wetted perimeter and cross sectional area of each channel, respectively.

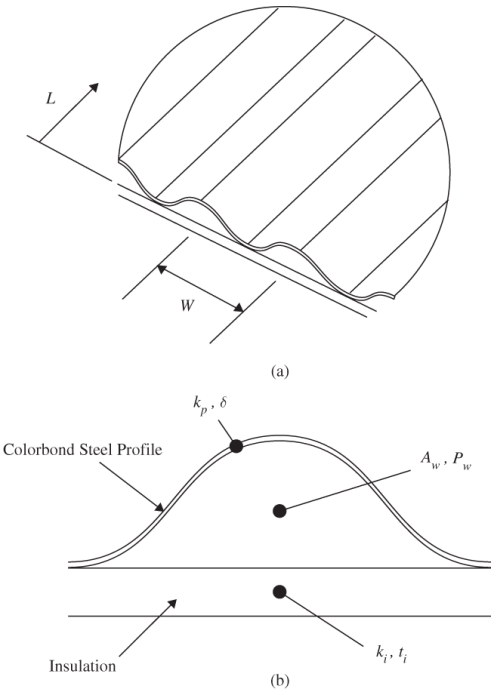

Fig. 3. The energy balance on the unglazed solar collector with colorbond steel absorber plates. G (W/m^2) is the solar radiation incident on the solar collector per unit area, which is absorbed by the absorber plate inclined at an angle, θ, to the horizontal; α_p (dimensionless) is the absorptivity of the absorber plate; T_p (K) is the mean absorber plate temperature; T_f (K) is the mean water temperature across the channel section perpendicular to the flow direction; T_∞ (K) is the ambient air temperature; u_w (m/s) is the average wind speed; h_r (W/m^2·K) is the heat loss coefficient through thermal radiation from the absorber plate to the sky; h_w (W/m^2·K) is the heat loss coefficient through convection by wind; h_b (W/m^2·K) is the heat loss coefficient through conduction across the back insulation; and Q_u (W) is the useful heat gain, respectively.

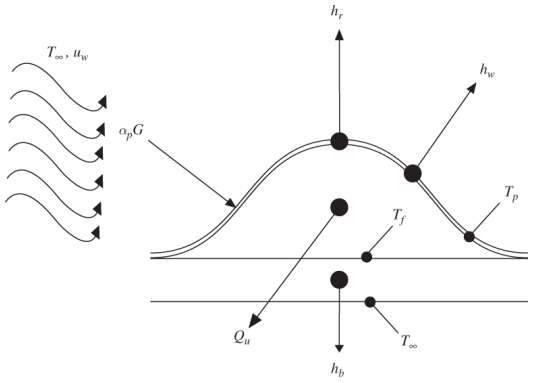

Fig. 4. The two types of unglazed solar collectors with colorbond steel absorber plates modelled by the sheet-tube model (Duffie and Beckman, 1980).

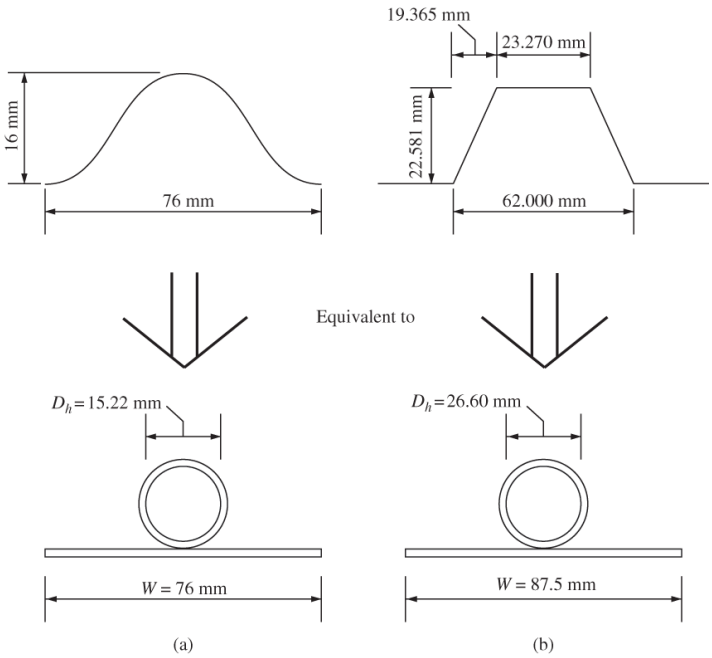

Fig. 5. Thermal network for the unglazed solar collectors with colorbond steel absorber plates: (a) in terms of conduction, convection, and radiation resistances; (b) in terms of resistances between the sky and the bottom of the back insulation.

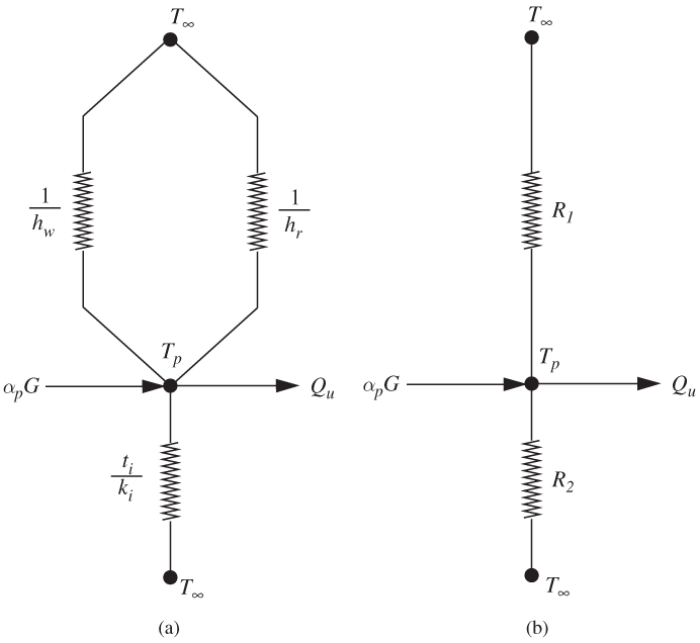

Fig. 6. Equivalent thermal network for the unglazed solar collectors with colorbond steel absorber plates.

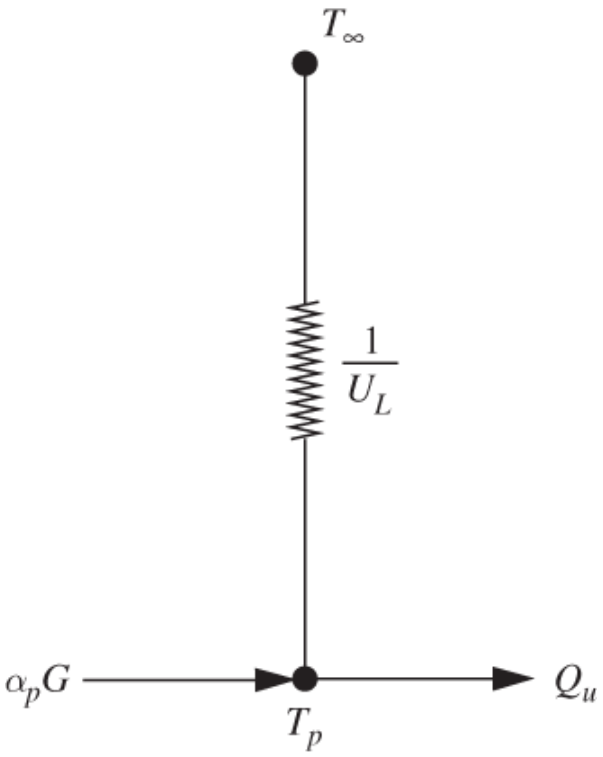

Fig. 7. Schematic of the solar water heating system showing the connection between the solar collector and the storage tank and the major parameters affecting the system's thermal performance. M_s (kg) is the total mass of water in the storage tank.

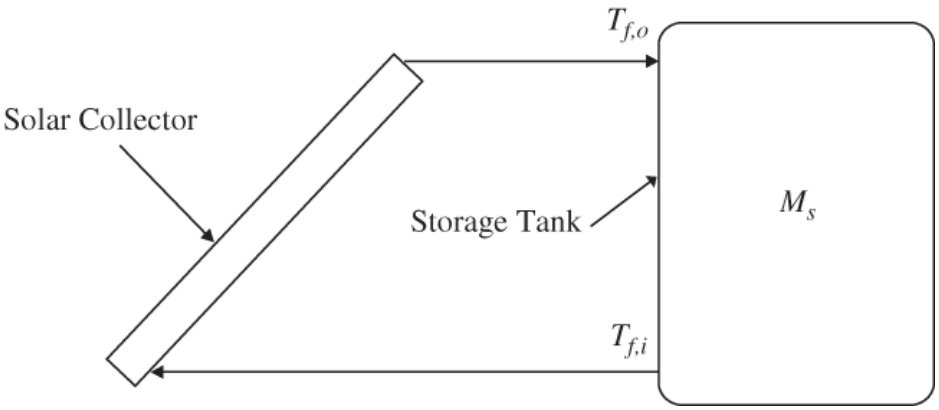

Fig. 8. The "push in – push out" model used to represent the vertical distribution of water temperature within the storage tank during the successive five-minute interval of calculations, where $T_{f,i}^{m}$ (K) is the water temperature at segment m.

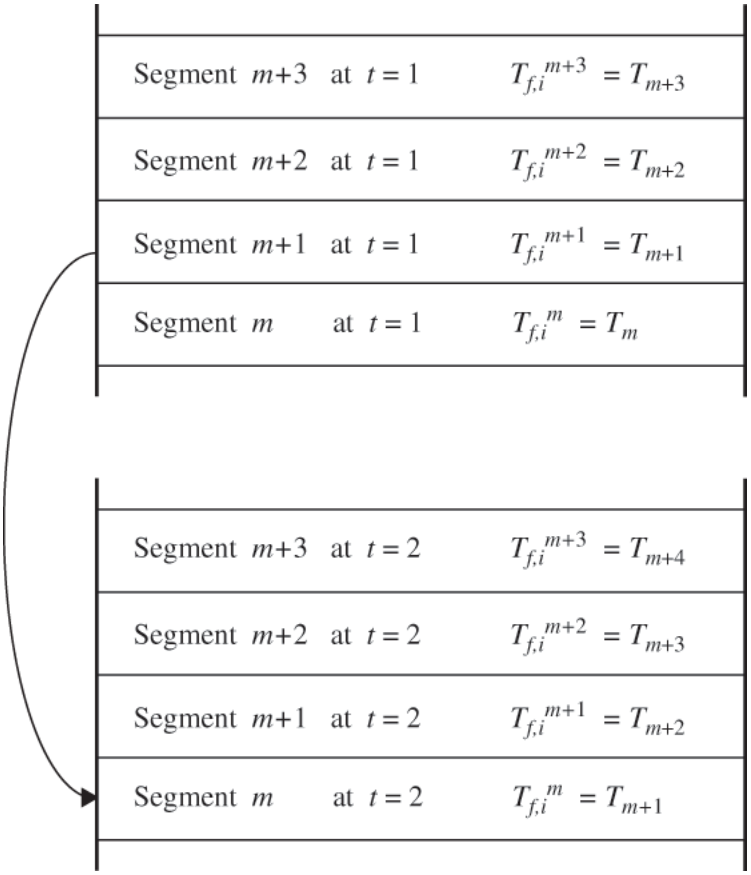

Fig. 9. Calculated results demonstrating the effect of ε_p on the thermal performance of both types of collectors: (a) η vs ε_p; (b) $T_{f,o}$ vs ε_p; (c) ΔT_f vs ε_p; and (d) T_p vs ε_p.

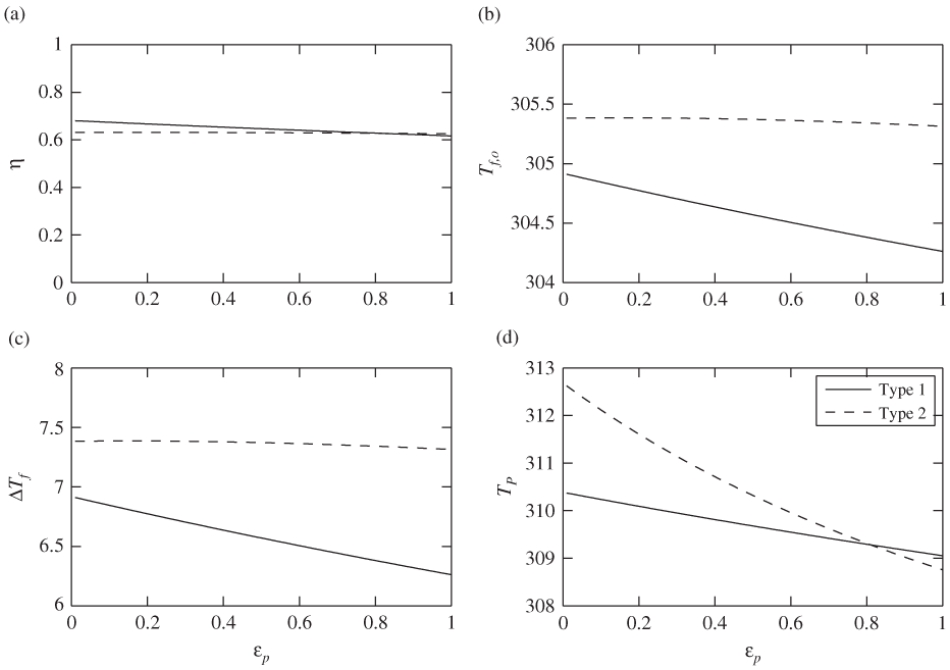

Fig. 10. Calculated results demonstrating the effect of α_p on the thermal performance of both types of collectors: (a) η vs α_p; (b) $T_{f,o}$ vs α_p; (c) ΔT_f vs α_p; (d) T_p vs α_p.

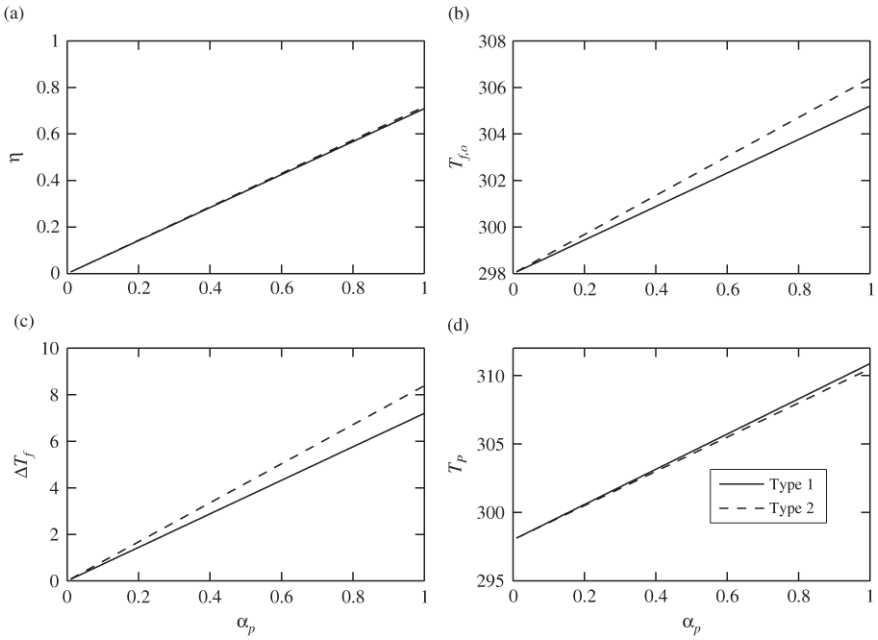

Fig. 11. Calculated results demonstrating the effect of n on the thermal performance of both types of collectors: (a) η vs n, (b) $T_{f,o}$ vs n, (c) ΔT_f vs n, (d) T_p vs n.

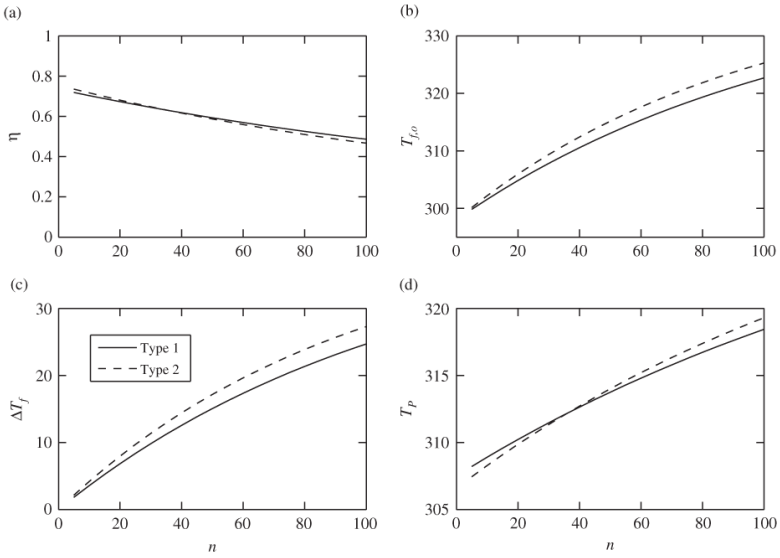

Fig. 12. Calculated results demonstrating the effect of M_s in the range of 100 - 800 kg on the thermal performance of Type 1 collector: Time series of $T_{f,i}$ (a), $T_{f,o}$ (b), η (c), and ΔT_f (d).

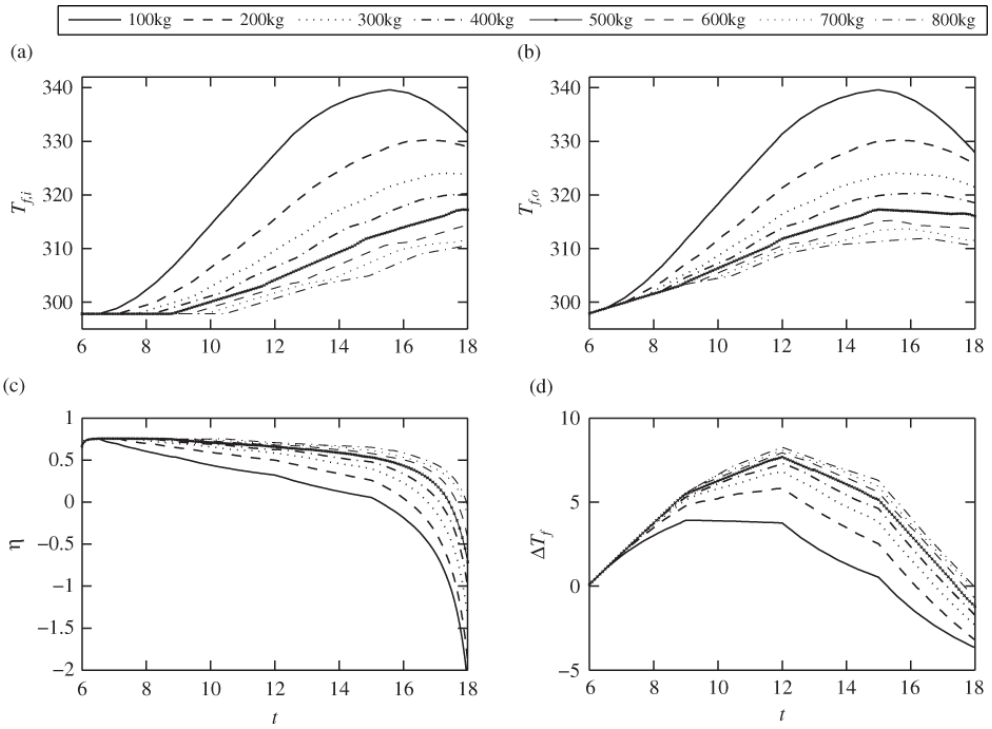

Fig. 13. Calculated results demonstrating the effect of M_s in the range of 100 - 800 kg on the thermal performance of Type 2 collector: Time series of $T_{f,i}$ (a), $T_{f,o}$ (b), η (c), and ΔT_f (d).

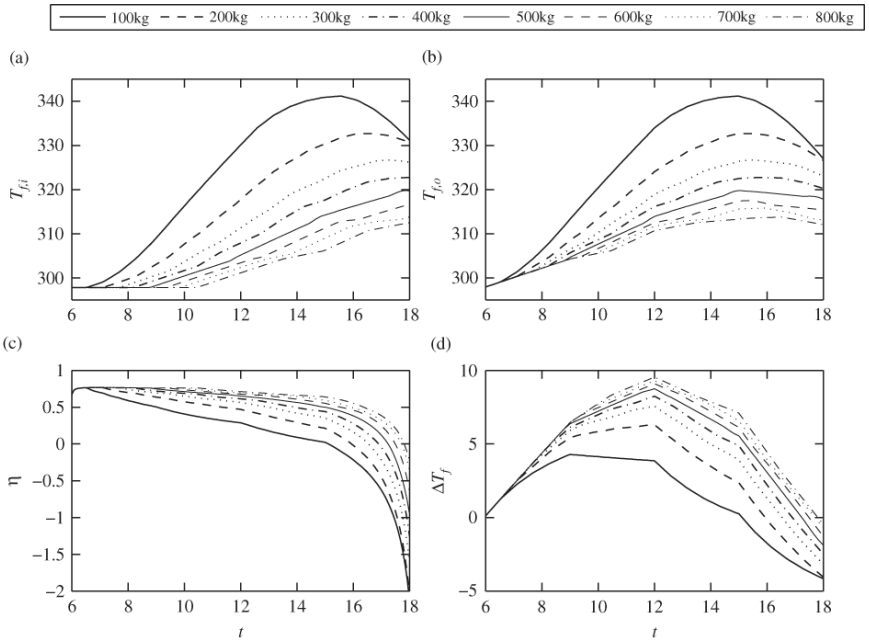

Fig. 14. Calculated results demonstrating the effect of G on the thermal performance of both types of collectors: (a) η vs $\dot{m}$; (b) $T_{f,o}$ vs $\dot{m}$; (c) ΔT_f vs $\dot{m}$; and (d) T_p vs $\dot{m}$.

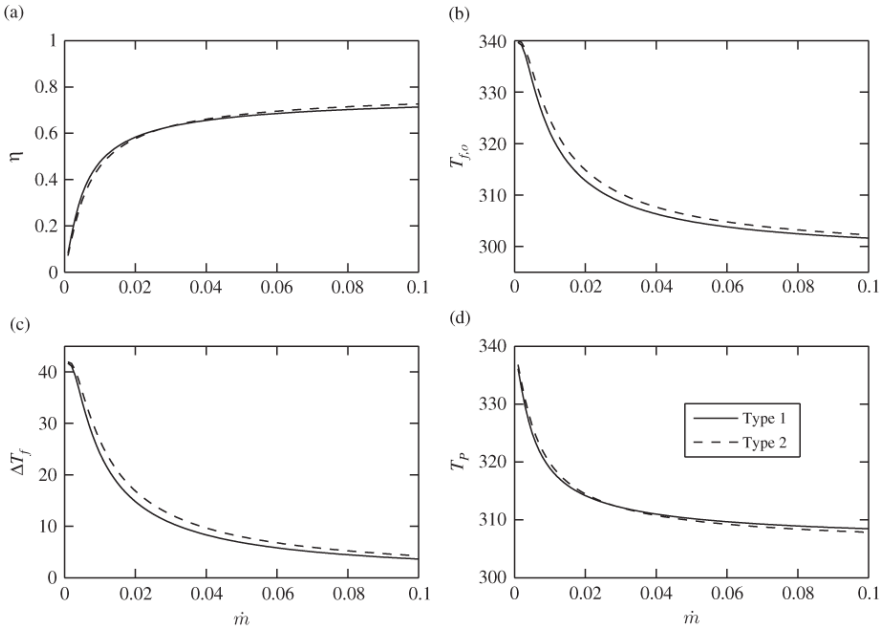

Fig. 15. Calculated results demonstrating the effect of G on the thermal performance of both types of collectors: (a) η vs $T_{f,i}$; (b) $T_{f,o}$ vs $T_{f,i}$; (c) ΔT_f vs $T_{f,i}$; and (d) T_p vs $T_{f,i}$.

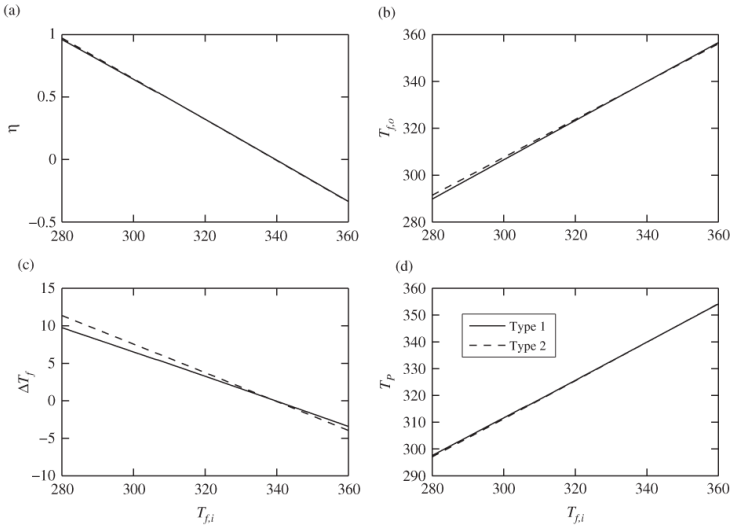

Table 1. Constants for calculating the Nusselt number at different Prandtl numbers

Prandtl Number	*a*	*b*	*c*	*d*
0.7	0.0791	0.0331	1.15	0.82
5	0.0534	0.0335	1.15	0.82
∞	0.0461	0.0316	1.15	0.84

Table 2. Monthly average total solar radiation on an hourly basis for each month of a year in Townsville (Australian Solar Energy Society, 2006).

Hour	Jan	Feb	Mar	Apr	May	Jun	Jul	Aug	Sep	Oct	Nov	Dec	Year
5													
6	10									19	51	44	10
7	177	138	122	93	59	32	27	68	152	206	231	227	128
8	343	300	303	262	212	188	186	244	343	394	412	411	300
9	510	462	484	432	364	345	347	421	535	582	593	595	472
10	608	573	589	520	446	434	445	522	650	698	687	698	572
11	706	684	695	610	527	524	543	623	766	814	782	801	673
12	804	795	800	699	609	613	641	725	882	930	877	904	773
13	757	744	735	631	543	546	579	658	794	835	804	835	705
14	710	693	669	562	478	480	517	592	705	740	731	767	637
15	664	643	604	495	412	413	455	526	618	646	659	698	569
16	481	461	418	328	259	257	291	348	412	435	454	497	387
17	299	279	233	161	107	101	128	170	207	224	250	295	205
18	117	97	48	3					2	14	46	94	35
Daily	22.3	21.1	20.5	17.3	14.5	14.2	15.0	17.6	21.8	23.5	23.7	24.7	19.7

Table 3. Monthly average highest, average, and lowest temperatures at 9am and 3pm respectively for each month of a year in Townsville (Australian Solar Energy Society, 2006).

Time	Monthly average temperature (°C)	Jan	Feb	Mar	Apr	May	Jun	Jul	Aug	Sep	Oct	Nov	Dec
9am	Highest	29.6	28.6	28.0	26.2	23.8	21.6	21.1	22.0	25.1	27.0	28.0	29.6
	Average	28.5	28.0	27.3	25.6	23.1	19.8	19.1	21.2	24.0	26.0	27.6	28.8
	Lowest	25.6	26.3	26.4	25.0	22.1	17.7	17.8	20.5	22.8	25.1	26.7	27.8
3pm	Highest	31.3	30.7	30.5	28.7	27.0	24.8	24.5	25.4	27.2	29.3	29.7	31.3
	Average	30.0	30.0	29.5	28.1	26.2	24.1	23.3	24.4	26.3	27.8	29.1	30.5
	Lowest	26.4	27.8	28.7	27.4	25.4	23.2	22.6	23.5	25.6	27.0	28.4	29.4

Table 4. Monthly average highest, average, and lowest wind speeds for each month of a year in Townsville (Australian Solar Energy Society, 2006).

Wind Speed (m/s)	Jan	Feb	Mar	Apr	May	Jun	Jul	Aug	Sep	Oct	Nov	Dec
Highest	3.3	3.7	3.2	3.9	2.5	2.9	3.0	4.2	4.2	4.7	4.0	4.4
Average	2.7	2.8	2.5	2.5	2.2	2.0	2.4	2.9	3.1	3.3	3.2	3.1
Lowest	2.2	1.7	2.1	1.5	1.8	1.1	2.0	2.1	2.2	2.6	2.2	1.7

Table 5. Calculated results for the thermal performances of both types of collectors under typical configurations and operating conditions

Parameter	Type 1 collector	Type 2 collector
η	0.6924	0.6976
Q_u (W)	1473.5	1709.0
$T_{f,o}$ (K)	305.03	306.16
T_p (K)	309.37	309.15
ΔT_f (K)	7.03	8.16
F_R	0.7289	0.7343
F'	0.7978	0.8165